Chinese Journal of
POLYMER SCIENCE

RESEARCH ARTICLE

https://doi.org/10.1007/s10118-026-3863-7
Chinese J. Polym. Sci.

Chlorosulfonated Poly(propylene carbonate) as High-performance Hot-melt Adhesives: Balancing Interfacial Adhesion and Cohesive Strength through Molecular Weight Window Engineering

Hai-Long Tian, Meng-Yu Yang, Hai-Ying Tan, Jing Jin*, Yun-Bao Gao*, and Wei Jiang*

State Key Laboratory of New Textile Materials and Advanced Processing Technologies and Key Laboratory of Textile Fiber and Products of Ministry of Education, College of Materials Science and Engineering, Wuhan Textile University, Wuhan 430200, China

Electronic Supplementary Information

Abstract The concurrent realization of high adhesion strength, biodegradability, and solvent-free processing in hot-melt adhesives (HMAs) is a persistent material design challenge. This study reports a gas-solid phase chlorosulfonation of poly(propylene carbonate) (PPC) with sulfuryl chloride, which installs polar functional groups while inducing controlled main-chain degradation, yielding chlorosulfonated PPC (CSPPC) with precisely tunable molecular weights. This dual chemical modification synergistically enhanced both interfacial adhesion and cohesive strength. The optimized CSPPC-35 ($\overline{M_n}$=35 kg/mol) achieves a single lap shear adhesion of 6.35 MPa on stainless steel, a peel strength of 131 N/cm, and durable adhesion of 99 h, exhibiting a transition from interfacial to cohesive failure attributed to a balanced viscoelastic state ($G'\approx G''\approx 10^5$ Pa). Subsequent chain extension with poly(butylene adipate-*co*-terephthalate) (PBAT)/4,4′-diphenylmethane diisocyanate (MDI) further elevates the adhesion strength to 14.23 MPa. Systematic rheological studies revealed that a narrow molecular weight window (30–35 kg/mol) of CSPPC is essential for balancing elastic recovery and viscous dissipation. This study circumvents the conventional HMA paradigm reliant on small-molecule polymerization by leveraging chlorosulfonation as a dual-functional post-polymerization modification of CO_2-derived PPC, concurrently introducing polar functionalities and inducing controlled main-chain scission to enable simultaneous polarity enhancement and molecular weight tuning. This strategy establishes the CSPPC as a scalable platform for sustainable, high-performance CO_2-derived HMAs.

Keywords Hot-melt adhesive; Poly(propylene carbonate); Rheology; Chlorosulfonation; CO_2 circular economy

Citation: Tian, H. L.; Yang, M. Y.; Tan, H. Y.; Jin, J.; Gao, Y. B.; Jiang, W. Chlorosulfonated poly(propylene carbonate) as high-performance hot-melt adhesives: balancing interfacial adhesion and cohesive strength through molecular weight window engineering. *Chinese J. Polym. Sci.* https://doi.org/10.1007/s10118-026-3863-7

INTRODUCTION

Hot-melt adhesives (HMAs) are thermoplastic polymer materials that remain solid at room temperature, are applied in molten form following thermal activation, and achieve rapid, cohesive bonding upon cooling and solidification.[1,2] HMAs are extensively employed across industrial sectors, including packing, electronics, construction, healthcare, and wood-based sandwich panel manufacturing. However, most HMAs currently employed in industrial applications are synthesized from petroleum-derived polymers, including polyurethanes,[3–6] polyolefins,[7,8] and polyamides.[9,10] High-strength variants typically depend on the irreversible crosslinking mechanism in thermosetting resins[11] or dynamic covalent network in thermoplastic systems.[12] Thermosetting HMAs exhibit permanent covalent network architectures and intrinsic resistance to biodegradation, rendering them environmentally persistent following disposal.[13] Consequently, their accumulation exerts persistent ecological pressure and poses significant challenges to environmental sustainability and end-of-life management.[14] Conversely, conventional thermoplastic resins have intrinsically limited adhesion strength and long-term durability.[15] This fundamental incompatibility with green manufacturing principles and circular economy paradigms underscores the urgent need to develop sustainable, functionally competitive alternatives.[16,17] In recent years, intensified research efforts have been directed toward the development of bio-based,[18–20] biodegradable HMAs to address sustainability challenges. Notably, syndiotactic-rich poly(3-hydroxybutyrate) exhibits adhesion strengths surpassing those of its petroleum-based counterparts, achieving single-lap shear strengths exceeding 30 MPa in wood bonding applications.[21] These advancements demonstrate that biodegradability and high performance are critical for sustainable HMAs.[22–24] Nevertheless, developing

* Corresponding authors, E-mail: jjin@wtu.edu.cn (J.J.)
E-mail: ybgao@wtu.edu.cn (Y.B.G.)
E-mail: weijiang@wtu.edu.cn (W.J.)
Received July 22, 2026; Accepted August 25, 2026; Published online November 9, 2026

© Chinese Chemical Society
Institute of Chemistry, Chinese Academy of Sciences

biodegradable HMAs that simultaneously deliver robust mechanical properties and environmental compatibility *via* simple, scalable, and cost-effective processes, without relying on complex synthesis, remains a critical challenge for both academia and industry.[25–28]

Poly(propylene carbonate) (PPC) is a biodegradable polymer[29] synthesized *via* the alternating copolymerization of carbon dioxide and propylene oxide.[30,31] It exhibits a glass transition temperature in the range of approximately 30–40 °C. However, its practical application is hindered by several inherent limitations, including poor thermal stability at elevated temperatures, pronounced low-temperature brittleness, and inferior surface affinity.[32] Furthermore, the intrinsically low cohesive strength of PPC results in a weak adhesive performance, significantly restricting its broader adoption in adhesive applications. In previous studies, chlorine atoms were introduced onto PPC molecular chains through gas-solid phase chlorination to yield chlorinated PPC (CPPC),[33–35] endowing the polymer with intrinsic adhesive functionality while retaining its biodegradability for HMA applications. The resultant CPPC achieved a wood-bonding shear strength of up to 7.4 MPa,[29] exceeding that of conventional ethylene-vinyl acetate-based HMAs. To further improve performance, CPPC was subsequently chain-extended, yielding HMA formulations with enhanced cohesive strength and markedly improved water resistance.[35]

Moreover, polar functionalities, specifically sulfur and chlorine atoms, were introduced onto PPC chains *via* a liquid-solid phase chlorosulfonation to synthesize chlorosulfonated PPC (CSPPC) for pressure-sensitive adhesive (PSA) applications.[36] The resultant CSPPC exhibited a peeling strength of 4.4 N/cm, marginally surpassing that of commercial Duct Tape® (3M 2929) at 4.1 N/cm.[37] Unlike these studies, which targeted PSAs functioning at room temperature, the present work focuses on hot-melt adhesives and, for the first time, systematically establishes the structure and property relationship between the molecular weight of CSPPC and its adhesion performance while effectively mitigating the degradation issue caused by residual low-molecular-weight fractions, ensuring the long-term stability required for practical applications. Furthermore, an optimal molecular weight window is identified which provides a definitive design criterion absent in the previous works.

This study circumvents the conventional HMA paradigm reliant on small-molecule polymerization, instead of leveraging chlorosulfonation as a dual-functional post-polymerization modification of CO_2-derived PPC. This *in situ* transformation concurrently introduces highly polar functionalities and induces controlled main-chain scission, enabling simultaneous polarity enhancement and precise molecular weight tuning. The structure-property relationships among the CSPPC molecular weight, chlorine/sulfur content, and adhesive performance were systematically elucidated. By integrating the bulk tensile mechanical properties with dynamic rheological data, the underlying mechanism governing how the molecular chain architecture intrinsically dictates the ultimate performance of HMAs was further revealed. Using CSPPC as a versatile precursor, a series of HMAs were synthesized *via* chain-extension reactions, demonstrating consistently high bonding strengths across diverse substrates and multiple chain-extender chemistries. These results validate CSPPC as a robust, general-purpose precursor for high-performance HMAs.

EXPERIMENTAL

Materials

PPC was obtained from the Changchun Institute of Applied Chemistry (Changchun, China). SO_2Cl_2 and 4,4′-diphenylmethane diisocyanate (MDI) were purchased from Macklin Biochemical Technology Co., Ltd. (Shanghai, China). Poly(butylene adipate-*co*-terephthalate) (PBAT) was supplied by Sida Polymer Materials Company (Chengdu, Sichuan, China). Polycaprolactone (PCL) was obtained from Solvay (PCL-6500). All the purchased chemicals were used as received without further purification.

Sample Preparation

Preparation of CSPPC

CSPPCs were synthesized *via* a gas-solid phase reaction method without any catalyst. PPC powder and SO_2Cl_2 at different molar ratios were added to the two three-necked flasks. The temperature of the vaporization unit was set at 110 °C, the reaction unit was maintained at 90 °C, and the chlorosulfonation reaction was carried out for 120 min. After reaction, the samples were removed and cooled to room temperature. Based on the molecular weight differences of the obtained CSPPCs, they were designated as CSPPC-54, CSPPC-49, CSPPC-35, CSPPC-30, and CSPPC-14, respectively. The products were purified by dissolution (trichloromethane) followed by recrystallization *via* the dropwise addition of ethanol.

Preparation of CSPPC-PBAT

According to different weight ratios, CSPPC and PBAT powders together with a certain amount of the chain extender MDI were introduced into a torque rheometer (XSS-300, Shanghai Ke Chuang rubber and plastic machinery equipment Co., Ltd., China) to induce the chain extension reaction. A mixture of the three components was compounded at 140 °C for 5 min. After the reaction, the product was removed from the rheometer and allowed to cool naturally to room temperature under ambient conditions. The purification procedure was as follows: the product was first dissolved in trichloromethane, followed by recrystallization *via* the dropwise addition of ethanol. Using the same procedure, the reaction of CSPPC with MDI and the chain extension reactions of CSPPC with PPC, CPPC, and PCL were also performed.

CSPPC Characterization

Fourier transform infrared spectroscopy (FTIR)

Fourier transform infrared spectroscopy (FTIR, Bruker Tensor II) was used to characterize the structure of the CSPPC. Purified CSPPC samples were hot-pressed into thin films, and spectra were collected in transmission mode with 32 scans over a wavenumber range of 400–4000 cm^{-1} at a resolution of 8 cm^{-1}. CSPPC-PBAT, CSPPC-PCL, CSPPC-PPC, CSPPC-MDI, and CSPPC-CPPC were tested using the same procedure.

Nuclear magnetic hydrogen spectroscopy (^{1}H-NMR)

Purified CSPPC samples were characterized using a Bruker 400 MHz nuclear magnetic resonance spectrometer at room temperature with $CDCl_3$ as the solvent and tetramethylsilane (TMS)

https://doi.org/10.1007/s10118-026-3863-7

as the internal standard.

Thermogravimetric analysis (TGA)

TGA of CSPPC samples was performed using a Netzsch TG 209F1 thermal analyzer (Germany). The measurements were carried out under a nitrogen atmosphere by heating the samples from 30 °C to 600 °C at a heating rate of 10 °C/min.

Differential scanning calorimetry (DSC)

The glass transition temperature was determined using a differential scanning calorimeter (DSC 204F1, Netzsch, Germany) under a nitrogen atmosphere. The measurement procedure was as follows: the sample was first heated from −70 °C to 50 °C at a heating rate of 10 °C/min, held at 50 °C for 3 min, and then cooled to −50 °C at the same rate; subsequently, a second heating scan was performed from −70 °C to 50 °C at 10 °C/min, followed by another isothermal step for 3 min, and finally cooled to −70 °C. Based on the data from the second heating cycle, the thermal properties such as the glass transition temperature and crystallization temperature were analyzed, thereby obtaining the corresponding thermal transition information.

Gel permeation chromatography (GPC)

The relative molecular weights and distributions of the CSPPC samples were determined using gel permeation chromatography (GPC, Waters Alliance 2695). Tetrahydrofuran was used as the mobile phase at a flow rate of 1 mL/min, and the column temperature was set to 30 °C.

Elemental analysis

The chlorine content of the CSPPC was determined using a Dionex ICS-6000 ion chromatography system (Thermo Scientific, USA), while the sulfur content was determined using a Vario EL Cube elemental analyzer (Elementar, Germany).

Single lap shear strength

The bonding strength was determined by single-lap shear tests. According to ASTM D3165-07, the strength was evaluated using an M204C universal testing machine at 25 °C and a tensile rate of 10 mm/min. The lap joint consisted of two stainless steel substrates (dimensions: 20 mm × 85 mm; overlap area: 20 mm × 15 mm) with the sample placed between the two plates. Prior to testing, the joint was heated in a constant-temperature oven at 90 °C for 5 min, then removed and allowed to cool naturally to room temperature. A contact pressure of approximately 1.2 MPa was applied between the substrates by using two butterfly clips (32 mm). The reported results represent the average of the five tested specimens. Using the same method, the single lap shear strength of CSPPC on interfaces such as aluminum, walnut wood, and bamboo was tested.

For the chain-extended samples using CSPPC as the base material, prior to testing, the joint was heated in a constant-temperature oven at 140 °C for 5 min, then removed and allowed to cool naturally to room temperature. A contact pressure of approximately 1.2 MPa was applied between the substrates by using two butterfly clips (32 mm). The reported results represent the average of five specimens. CSPPC-MDI, CSPPC-PCL, CSPPC-PPC, and CSPPC-CPPC were tested using the same procedure. Using the same method, the single lap shear strength of CSPPC-PBAT on interfaces such as aluminum, walnut wood, and bamboo was tested.

Mechanical properties

According to the GB/T 1040.1-2006 standard, tensile tests were conducted on the CSPPC samples using an Instron 1121 material testing machine to evaluate their mechanical properties. The tests were performed at 25 °C at a tensile rate of 50 mm/min. The specimens were dumbbell-shaped, with a total length of 75 mm, narrow section width of 4 mm, and thickness of 2 mm. CSPPC-PBAT were tested using the same procedure.

Rheological tests

The rheological properties of the CSPPC samples were characterized using a parallel-plate rheometer (MCR-503, Anton Paar). The measurements were performed in oscillatory mode with a strain amplitude of 1%. Frequency sweep tests were conducted at 120 °C over a range of 0.01–100 Hz, while temperature sweep tests were carried out from 30 °C to 120 °C. Using the same procedure, temperature sweep tests of the CSPPC-PBAT samples were carried out over a temperature range of 30–140 °C.

180° peeling test

According to the ASTM D3330-04 standard, a PET film coated with CSPPC (width 2.5 cm) was adhered to a stainless steel plate surface using a 2 kg roller. The peel strength of the CSPPC was measured using an electronic peel tester (model BLD-200, Lab Think, China) at a peeling rate of 300 mm/min. The reported results represent the average of three parallel tests.

Shear resistance test

According to the ASTM D3654-06 standard, a PET film coated with CSPPC (width 2.5 cm) was adhered to a stainless-steel plate surface with a contact area of 25 mm × 25 mm using a 2 kg roller. Subsequently, a 1 kg weight was suspended from the free end of the film at 25 °C. The shear holding time is defined as the duration during which the CSPPC can withstand the load. The reported results represent the average of three parallel tests.

RESULTS AND DISCUSSION

Synthesis and Structural Characterization of CSPPC with Well-defined Structure

In this study, five CSPPC samples with gradient molecular weights were synthesized by precisely regulating the molar ratio of PPC to sulfuryl chloride and employing a two-step "sulfuryl chloride vaporization gas-solid phase chlorosulfonation" reaction protocol. The feed molar ratios, measured number-average and weight-average molecular weights, glass transition temperatures (T_g), and chlorine and sulfur elemental contents of each batch are summarized in Table 1.

As shown in Table 1, with increasing sulfuryl chloride feed molar ratio, the number-average molecular weight ($\overline{M}_n$) and chlorine content of the CSPPC decreased monotonically, whereas the sulfur content followed a non-monotonic trend, declining initially and subsequently increasing. This observation reflects a dosage-dependent transition in the prevailing reaction pathway governed by the sulfuryl chloride concentration. At low feed ratios of sulfuryl chloride (1:25, PPC: SO_2Cl_2), chlorination and sulfonation occurred predominantly *via* electrophilic substitution on the PPC backbone, with negligible chain degradation and consequently only modest reductions in $\overline{M}_n$. In contrast, at high feed molar ratios (1:100), excess sulfuryl chloride drives extensive backbone scission of PPC, leading to a pronounced decrease in $\overline{M}_n$ and the formation of volatile or low-molecular-weight degradation byproducts that are deficient in both chlorine and sulfur, resulting in

https://doi.org/10.1007/s10118-026-3863-7

lower measured bulk elemental contents. Notably, the synthesis of CSPPC differs fundamentally from the step-growth polymerization of monomeric precursors characteristic of conventional HMAs. Instead, the two competing reactions proceed concurrently. A substitution reaction introduces polar functionalities (chlorine and sulfur moieties), and a degradation reaction induces main-chain scission of the PPC backbone. Consequently, for HMA applications, a moderate sulfuryl chloride feed molar ratio enables the synthesis of CSPPC exhibiting both sufficiently elevated molecular weight to confer cohesive strength and enhanced polar moiety density to promote interfacial adhesion.

The chemical structures of the as-synthesized CSPPC samples were characterized by FTIR and ^{1}H-NMR spectroscopy. The FTIR spectrum (Fig. 1a) reveals the emergence of new absorption bands at 1347 and 740 cm^{-1}, attributable to the symmetric stretching vibrations of the O=S=O and the C−Cl stretching vibration, respectively, confirming the successful chemical modification of PPC by sulfuryl chloride. The ^{1}H-NMR spectrum (Fig. 1b) exhibits three new resonance signals at δ=4.85, 4.55, and 4.05 ppm, which are assigned to the methine and methylene protons of $-CH(SO_2Cl)_{x1}Cl_{Y1}$ and $-CH_2(SO_2Cl)_{x2}Cl_{Y2}$ structural units, respectively. These assignments confirmed that CSPPC was the predominant product arising from the electrophilic substitution of hydrogen atoms along the PPC backbone. Additionally, the signal corresponding to the terminal methyl protons (peak 4, Fig. 1b) at δ=1.50 ppm exhibits markedly enhanced intensity in CSPPC relative to pristine PPC, indicating that chain scission of the PPC backbone occurs concomitantly with the chlorosulfonation reaction. Therefore, these spectroscopic findings corroborate the successful chlorosulfonation of PPC and demonstrate that

Table 1 Molecular weight characteristics, chlorination and sulfonation content and T_g of PPC and CSPPC.

Sample	The molar ratio of PPC:SO_2Cl_2	$\overline{M_n}$ (kg/mol)	$\overline{M_w}$ (kg/mol)	PDI	Cl content (wt%)	S content (wt%)	T_g (°C)
PPC	0	60	148	2.46	0	0	36
CSPPC-1	1:25	54	109	2.01	3.27	0.250	10
CSPPC-2	1:37.5	49	82	1.67	3.00	0.195	8
CSPPC-3	1:50	35	68	1.94	1.44	0.185	4
CSPPC-4	1:75	30	44	1.46	0.72	0.210	−2
CSPPC-5	1:100	14	25	1.78	0.60	0.445	−5

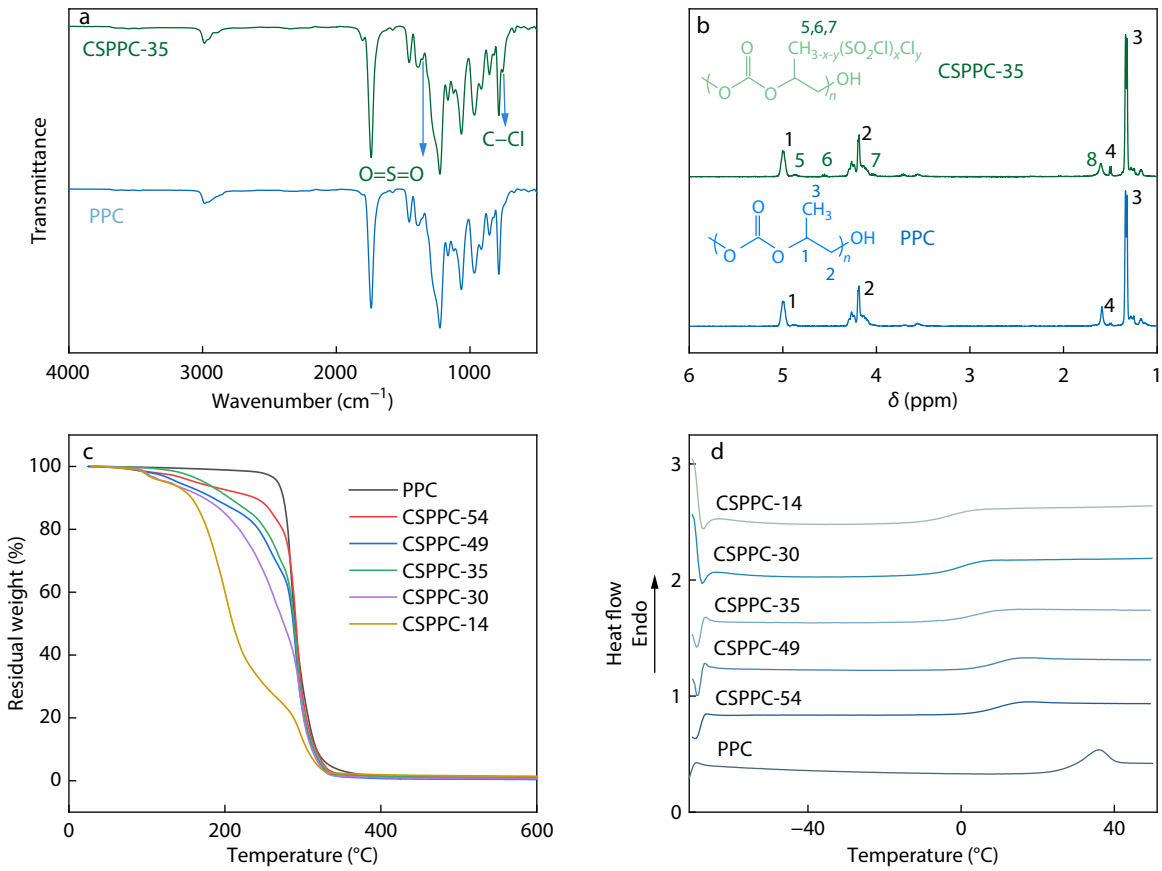


Fig. 1 (a) FTIR spectra of PPC and CSPPC-35; (b) ^{1}H-NMR spectra of PPC and CSPPC-35; (c) TGA thermograms of PPC and CSPPC with different molecular weights; (d) DSC curves of the second heating melting process of PPC and CSPPC with different molecular weights.

https://doi.org/10.1007/s10118-026-3863-7

this chemical modification is accompanied by a controlled main-chain degradation.

The thermal stability of the PPC and CSPPC samples was evaluated using TGA and DSC. TGA was employed to assess the decomposition profiles and onset temperatures (Fig. 1c), while DSC was used to determine T_g and detect any thermal transitions indicative of degradation (Fig. 1d). As depicted in Fig. 1(c), CSPPC exhibits a markedly reduced thermal degradation temperature relative to pristine PPC, dropping from 291 °C to as low as 197 °C with the magnitude of decrease correlating strongly with the extent of molecular weight reduction. These findings indicate that chlorosulfonation severely undermines the thermal stability of PPC and that the degree of destabilization is directly governed by the extent of polymer chain scission. As presented in Fig. 1(d) and summarized in Table 1, T_g of CSPPC decreases monotonically from 10 °C to −5 °C as the number-average molecular weight ($\overline{M}_n$) decreases from 54 kg/mol to 14 kg/mol. In contrast, pristine PPC exhibited a T_g of 36 °C. This pronounced T_g depression arises from a combination of main-chain degradation and side-group plasticization, with the effect of scaling inversely proportional to the degree of polymerization.

Overall, FTIR and ^{1}H-NMR analyses confirmed the successful synthesis of the CSPPC samples with well-defined molecular weights. Thermal characterization indicated that chlorosulfonation substantially compromised the thermal stability of PPC and resulted in a concomitant reduction in T_g. Crucially, this scission is not merely a side effect but a tunable parameter. By precisely balancing the extent of chain cleavage against the degree of polar group incorporation (*e.g.*, $-SO_2Cl$ and $-Cl$), the cohesive energy density and interfacial adhesion capability of CSPPC can be rationally engineered at the molecular level. This dual-parameter control enables the tailoring of CSPPC's thermomechanical profile, thereby establishing a robust structural and performance basis for its use as a high-performance HMA precursor.

The Relationship between Adhesive Performance of CSPPC and Its Bulk Mechanical Properties and Rheological Behavior

To evaluate the feasibility of CSPPC as a high-performance HMA precursor, this section evaluates its adhesive and mechanical properties, focusing on how the molecular structure governs the lap shear strength on stainless steel substrates. Specifically, the correlations between the number-average molecular weight, combined content of chlorine and sulfur, and adhesive performance were examined to establish the molecular design criteria required for optimizing the cohesive strength and interfacial adhesion (Fig. 2). The nomenclature of CSPPC follows a systematic convention wherein distinct designations correspond to specific ranges of $\overline{M}_n$.

As illustrated in Fig. 2(a), the single-lap shear strength of CSPPC exhibits a non-monotonic dependence on $\overline{M}_n$, increasing initially and subsequently decreasing upon further chain shortening. All CSPPC samples underwent cohesive failure within the adhesive layer when bonded to stainless-steel substrates (Fig. 2b; representative image shown for CSPPC-35). The optimal adhesive performance was achieved by CSPPC-35 ($\overline{M}_n$=35 kg/mol), which exhibited a maximum single lap shear strength of 6.35 MPa at chlorine and sulfur contents of 1.44 wt% and 0.185 wt%, respectively (Figs. 2a and 2c).

Notably, the CSPPC-35 sample exhibited cohesive failure when bonded to a stainless-steel substrate, indicating that in-

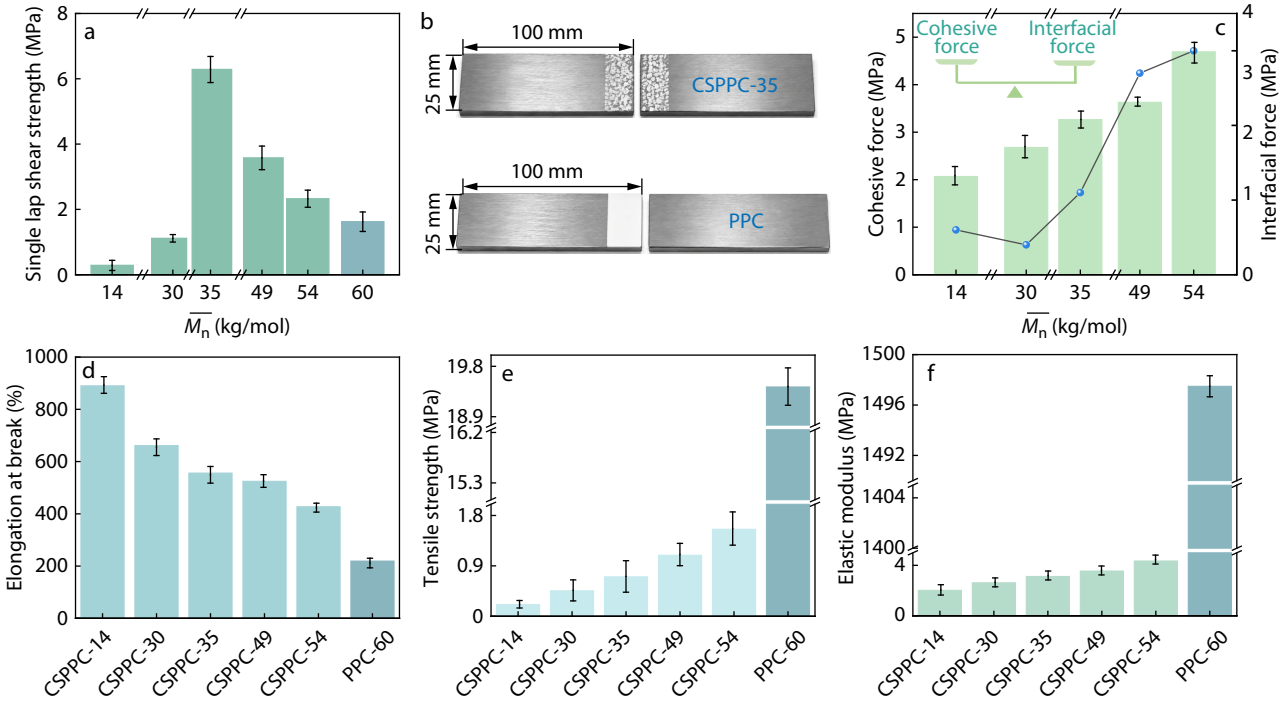


Fig. 2 (a) Single lap shear strength of CSPPC on stainless steel substrates; (b) Failure modes of PPC and CSPPC-35 at the stainless steel substrate interface; (c) Relationship between CSPPC with different molecular weights and elastic modulus (cohesive component) as well as total chlorine and sulfur content (polarity component); (d) Elongation at break, (e) tensile strength, and (f) elastic modulus of CSPPC with different molecular weights.

https://doi.org/10.1007/s10118-026-3863-7

terfacial adhesion exceeded the internal cohesive strength of the polymer matrix. In contrast, pristine PPC ($\overline{M_n}$=60 kg/mol) failed at the metal-adhesive interface (Fig. 2b). This transition from interfacial failure in pristine PPC to cohesive failure in the optimized CSPPC sample provides definitive evidence of robust interfacial bonding and represents a critical prerequisite for high-performance adhesive systems. Moreover, this transition is further corroborated by the tensile strength and elastic modulus data presented in Figs. 2(d)–2(f), both of which exhibit a monotonic decrease with the decreasing molecular weight of CSPPC. This inverse correlation between molecular weight and bulk mechanical properties confirmed that the cohesive strength of the adhesive layer diminished as chain scission progressed, thereby rationalizing the observed shift from cohesive failure (at intermediate molecular weights, *e.g.*, CSPPC-35, where interfacial adhesion still exceeds bulk strength) to potential interfacial or mixed failure modes at excessively low molecular weight values.

Furthermore, the adhesive performances of the pristine PPC and CSPPC were systematically evaluated through persistent adhesivity and peel strength measurements (Table 2). Pristine PPC exhibits negligible peel adhesion on the PET paper film and a holding power of only 2 h under a 1 kg load, reflecting its inherently poor cohesive strength and inadequate interfacial interaction with polar substrates. Upon chlorosulfonation, the adhesive properties were profoundly altered in a molecular weight-dependent manner. CSPPC-54 and CSPPC-49 demonstrated moderate improvements in holding power (9 and 8 h, respectively) and peeling strength (103 and 98 N/cm), attributable to the introduction of polar chlorosulfonyl groups that enhance substrate wetting and interfacial adhesion. Significantly, CSPPC-35 achieved an exceptional holding power of 99 h and peel strength of 131 N/cm, representing the optimal balance between the cohesive strength and interfacial adhesion within the investigated series. Conversely, further reduction in the molecular weight to 30 and 14 kg/mol resulted in a dramatic deterioration in both the holding power (10 h and 18 min, respectively) and peel strength (60 and 5 N/cm). The precipitous decline at low molecular weights is ascribed to insufficient chain entanglement and compromised cohesive integrity, which cannot be compensated for by the increased polarity of the chlorosulfonated moieties.

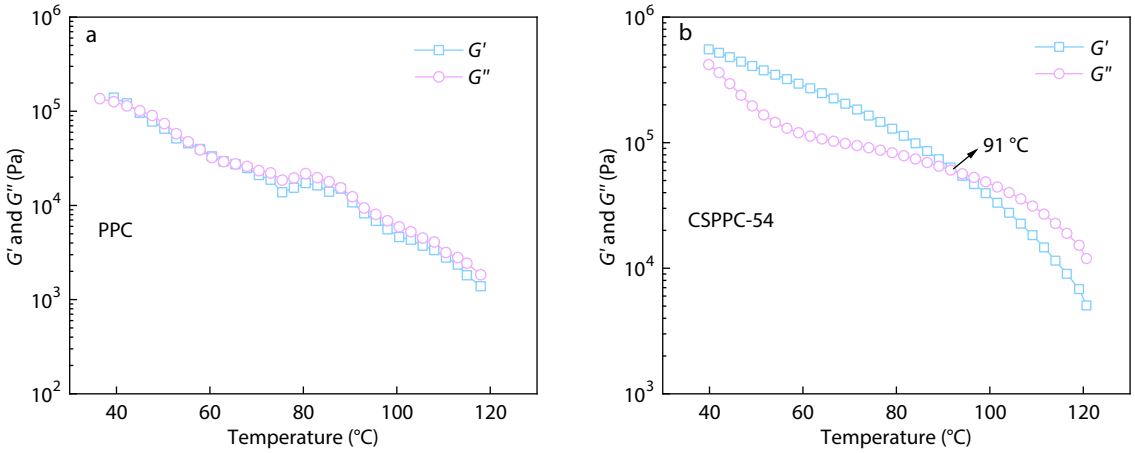
Table 2 Persistent adhesivity and peel strength of PPC and CSPPC with different molecular weights.

Sample	Persistent adhesivity 1 kg weight	Peel strength (N/cm) PET paper film
PPC	2 h	---
CSPPC-54	9 h	103
CSPPC-49	8 h	98
CSPPC-35	99 h	131
CSPPC-30	10 h	60
CSPPC-14	18 min	5

These findings collectively establish that the adhesive performance of CSPPC is governed by a molecular weight window effect, wherein an optimal degree of main-chain degradation during chlorosulfonation is essential to achieve the requisite viscoelastic balance for high-performance HMA.

To elucidate how the viscoelastic properties of CSPPC with various molecular weights influence hot-melt adhesive (HMA) performance, temperature-sweep rheological measurements were conducted to characterize the evolution of the storage modulus (G'), loss modulus (G''), and loss factor (tanδ) as a function of temperature for all formulations (Fig. 3). G' quantitatively reflects the elastic (solid-like) contribution and correlates directly with the cohesive strength, whereas G'' captures the viscous (liquid-like) response and is empirically associated with the interfacial energy dissipation and bond formation kinetics.[38] High-performance HMAs require not only high absolute magnitudes of both G' and G'', but also a favorable G'/G'' ratio within the service temperature window, thereby enabling the synergistic mechanical profile of "strength and adhesion", *i.e.*, robust internal integrity coupled with effective interfacial anchoring.[39]

As shown in Fig. 3(a), pristine PPC exhibits classic viscoelastic fluid behavior, and G' and G'' are nearly equivalent across the measured temperature range; however, both moduli remain low in absolute magnitude, indicating insufficient cohesive strength and poor interfacial adhesion. In contrast, the chlorosulfonated CSPPC samples with molecular weights above 35 kg/mol (Figs. 3b–3d) display a marked increase in both G' and G'' below the softening temperature, despite progressive molecular weight reduction. This counterintuitive enhancement demonstrates that chlorosulfonation introduces polar functionalities capable of reinforcing both intra-



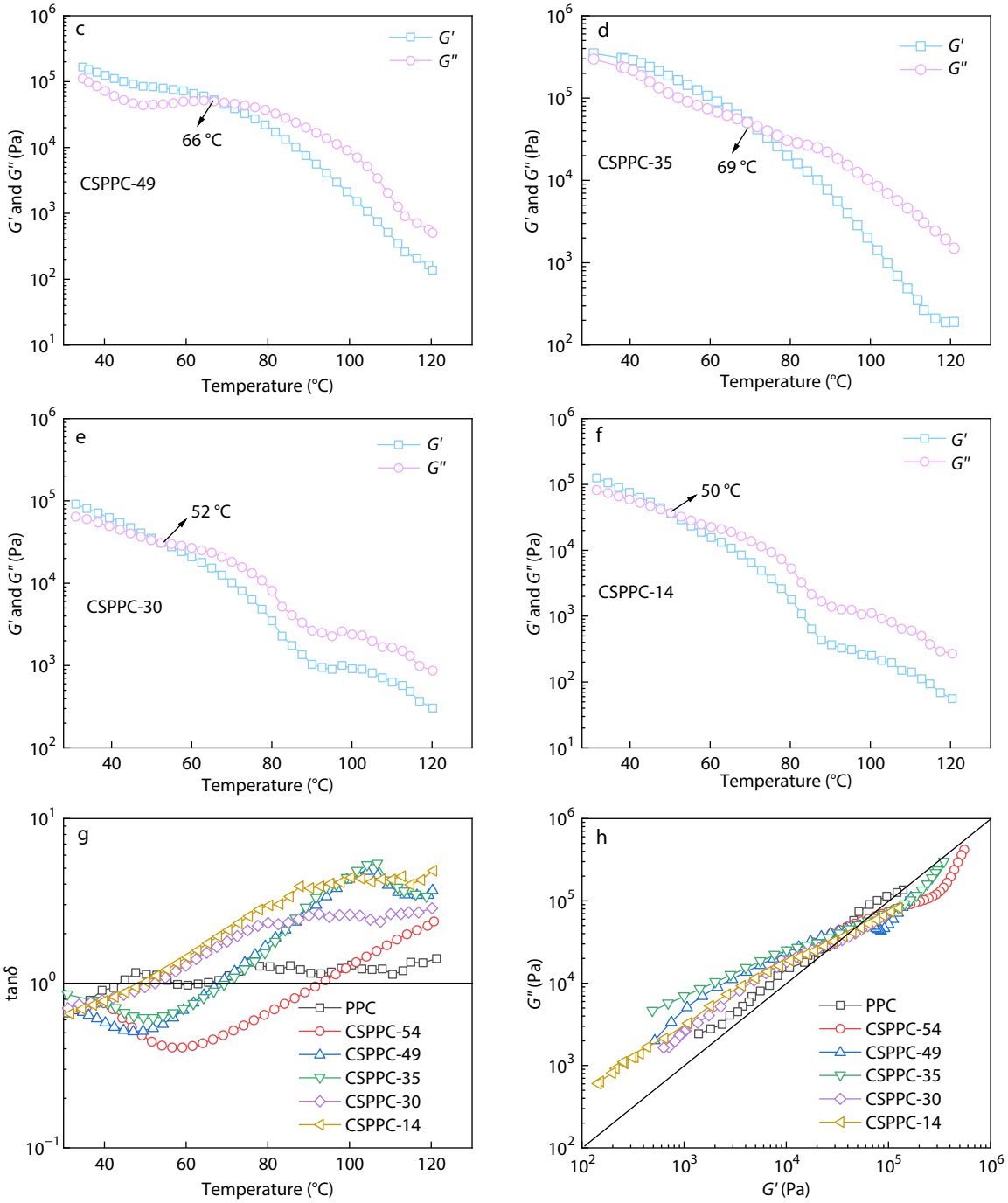


Fig. 3 Temperature sweep curves of PPC and CSPPC at 1% strain. (a) Storage modulus (*G*') and loss modulus (*G*'') of PPC; (b–f) Storage modulus (*G*') and loss modulus (*G*'') of CSPPCs; (g) Loss factor (tan*δ*) of CSPPCs; (h) Viscoelastic processing window of CSPPCs.

chain cohesion (*via* dipole-dipole interactions and potential crosslinking) and interfacial adhesion (*via* polar interactions with substrates), thereby achieving synergistic improvement in bulk and interfacial mechanical performance.

Significantly, CSPPC-35 ($\overline{M_n}$=35 kg/mol) was found to be the optimal formulation. Prior to softening, its *G*' and *G*'' converge at approximately 1.0×10^5 Pa, signifying a rare balanced high elasticity and high viscous dissipation, and collectively satisfy the dual rheological criteria for high-performance HMAs. This is sufficient melt strength for cohesive integrity during application and adequate energy dissipation for interfacial wetting and bond formation. In contrast, CSPPC-54 exhibited an elevated *G*′ but markedly suppressed *G*″ (Fig. 3b), reflecting excessive elasticity and inadequate energy dissipation, limiting interfacial wetting and bond formation. CSPPC-49 showed an improved *G*′/*G*″ balance but insufficient modulus magnitude overall, failing to deliver the required structural integrity and adhesive driving force. Below 35 kg/mol (Figs. 3e and 3f), both *G*′ and *G*″ undergo a sharp, irreversible decline, falling well outside the functional window for HMA

https://doi.org/10.1007/s10118-026-3863-7

application, confirming that excessive chain scission undermines the viscoelastic foundation necessary for effective melt processing and bond durability.

Moreover, the peak height of the loss factor (Fig. 3g) and temperature-dependent evolution of the G'/G'' ratio (Fig. 3h) collectively confirm that the CSPPC-35 sample exhibits superior bonding performance, high elasticity, and high viscosity, and fully satisfies the characteristic viscoelastic behavior expected of high-performance HMAs.

The Application of CSPPC as an HMA Precursor

In the previous section, we systematically elucidated the molecular weight-dependent structure and property relationships of CSPPC as hot-melt adhesive precursors. Rheological analysis revealed that CSPPC-35 balances the high elastic recovery with substantial viscous dissipation. This balanced viscoelastic state is consistent with the observed failure mode transition, from interfacial debonding (as observed for pristine PPC) to cohesive failure within the adhesive layer, indicating that the interfacial adhesion of CSPPC-35 has surpassed its own bulk cohesive strength, thereby establishing it as a highly promising candidate for high-performance hot-melt adhesive applications. Previous studies have employed PBAT as a second polymer phase to extend the PPC and chlorinated PPC, thereby enhancing the cohesive strength and substantially improving the adhesive performance. Building on these insights, this section further employs a chain-extension strategy to modify CSPPC-35. Specifically, PBAT reacted with CSPPC (Fig. 4) to enhance its bonding performance (Fig. 5a) and broaden its applicability across diverse substrate surfaces (Fig. 5b). Concurrently, to verify the generality of CSPPC as a versatile precursor and to validate the chain-extension strategy itself, systematic investigations were conducted on CSPPC modified with PBAT, PPC, and PCL (Figs. 4 and 5c). These comparative studies aimed to broaden the application scope of CSPPC as a thermoplastic adhesive precursor.

Specifically, the adhesion strength first increased with increasing molecular weight, peaked at CSPPC-35-PBAT, and then declined. This behavior is consistent with the adhesive performance of unmodified CSPPC (Fig. 2a), indicating that an optimal CSPPC chain length exists for balancing the cohesive integrity and interfacial adhesion energy in the CSPPC-PBAT system when deployed as a high-performance HMA. Notably, the CSPPC-35-PBAT conjugate achieved a maximum single-lap shear strength of 14.23 MPa (Fig. 5a), representing more than a two-fold enhancement over unmodified CSPPC-35 (6.35 MPa). The well-balanced G'/G'' ratio of CSPPC-35-PBAT shifts the failure mode from mixed (cohesive and interfacial) toward predominantly cohesive failure, indicative of optimized bulk energy dissipation and suppression of premature interfacial debonding. Conversely, CSPPC-PBAT systems derived from molecular weight extremes of 14 and 54 kg/mol exhibited substantially compromised adhesion, suggesting that deviations from the optimal chain length disrupt the synergistic balance between cohesive integrity and interfacial wettability requisite for high-performance bonding. Thus, the PBAT-modified chain extension of CSPPC is an effective strategy for enhancing the adhesion performance of hot-melt adhesives. The molecular weight of the unmodified CSPPC precursor remains the critical parameter governing the balance between cohesive strength and interfacial bonding, thereby establishing a universal molecular design criterion for CSPPC-based adhesive platforms.

Furthermore, the single lap shear strengths of pristine PPC, CSPPC-35, and CSPPC-35-PBAT were compared across four representative substrates: stainless steel, aluminum, walnut

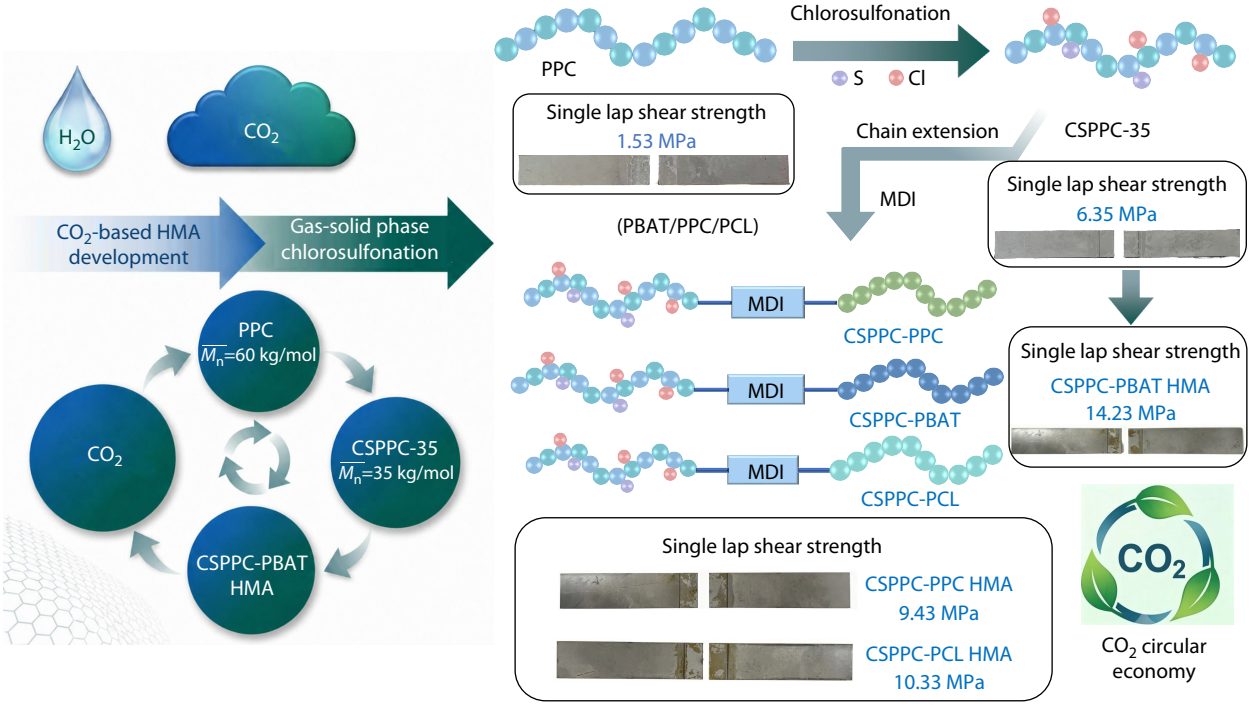


Fig. 4 The gas-solid phase reaction of PPC with SO_2Cl_2, the chain extension reactions of CSPPC with different materials and photographs of the fractured lap-shear specimens.

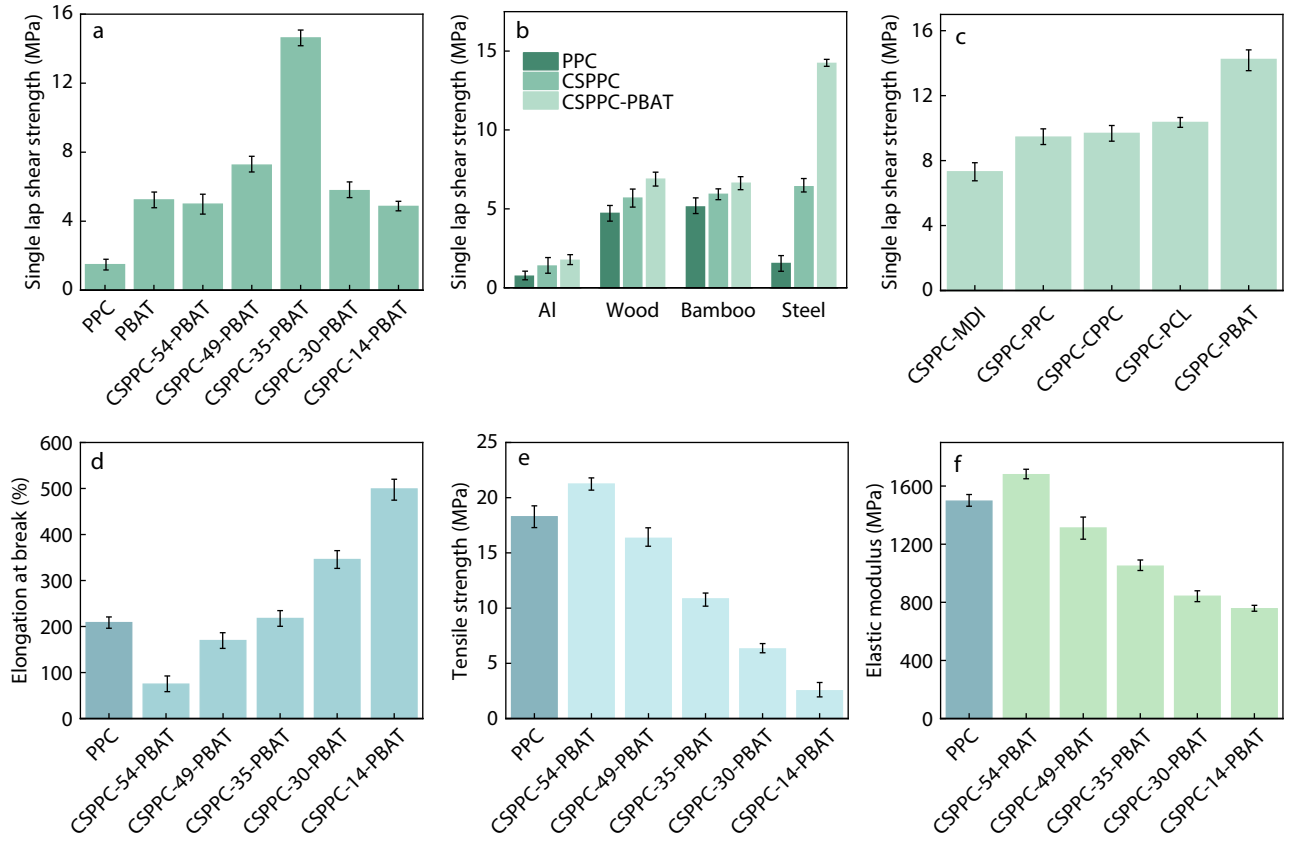


Fig. 5 Adhesion performance of the CSPPC adhesives; (a) Adhesion strength of CSPPC-PBAT hot-melt adhesives to stainless steel substrates; (b) Adhesion strength of PPC, CSPPC-35 and CSPPC-35-PBAT to various substrates; (c) Single lap shear strength of CSPPC chain-extended/crosslinked with PPC, CPPC, PCL at stainless steel interfaces; (d) Elongation at break, (e) tensile strength and (f) elastic modulus of CSPPCs-PBAT HMAs with varying molecular weights.

wood, and bamboo. As shown in Fig. 5(b), CSPPC-35 and CSPPC-35-PBAT both exhibited substantially superior adhesion strengths relative to pristine PPC on all tested substrates, with performance further enhanced following PBAT-modified chain extension. Notably, for the two lignocellulosic substrates, walnut wood and bamboo, the observed failure mode was cohesive failure within the substrate bulk, rather than interfacial debonding or adhesive disruption. This behavior demonstrates that the actual adhesion strength between CSPPC-35-PBAT and the wood-based materials exceeded the intrinsic cohesive strength of the substrates themselves. Consequently, the measured single-lap shear strength values represent the lower bounds of the true interfacial adhesion rather than the absolute performance limits. Although CSPPC-35-PBAT exhibits substrate cohesive failure on both wood and bamboo, the underlying interfacial interaction mechanisms differ markedly. For wood, which is rich in cellulose and thus possesses a high surface hydroxyl density, dense hydrogen bonds readily form between the substrate and the polar groups of CSPPC-35-PBAT. In addition, the loose and porous structure of wood allows adhesive penetration and anchoring, providing strong mechanical interlocking. However, bamboo relies mainly on interfacial polar adsorption, van der Waals forces and dipole interaction between the polar ester groups of the CSPPC-PBAT adhesives and the bamboo surface, coupled with the high bulk strength of the adhesive layer itself. These findings confirm that the CSPPC-PBAT system possesses exceptional interfacial bonding capability, enabling robust adhesion across diverse polar and non-polar substrates.

To investigate the universality of the aforementioned modification strategy, CSPPC-35 was employed as a reactive precursor and blended with four structurally distinct polymers (PPC, PBAT, CPPC, and PCL) in the presence of 5 wt% MDI. Detailed information regarding CSPPC-PPC, CSPPC-CPPC, and CSPPC-PCL is provided in Fig. S4 (in the electronic supplementary information, ESI). The single-lap shear strengths of the resulting copolymers on stainless-steel substrates were evaluated (Fig. 5c). All samples exhibited high adhesion performance, including the CSPPC-35 self-chain-extended system, with values exceeding that of unmodified CSPPC-35 (6.35 MPa). These results confirmed that CSPPC can efficiently react with diverse aliphatic and modified polyesters, underscoring its potential as a versatile high-performance HMA precursor.

This study further evaluated the elongation at break, tensile strength, and elastic modulus of CSPPC-PBAT formulations across a range of CSPPC molecular weights (Figs. 5d–5f). Relative to pristine PPC, all CSPPC-PBAT samples exhibited diminished elastic modulus and tensile strength, but substantially enhanced elongation at break. Specifically, the elongation at break increased systematically with decreasing molec-

ular weight of CSPPC, whereas the tensile strength and elastic modulus decreased monotonically. This trade-off between stiffness and ductility is a characteristic of thermoplastic elastomer design. The lower molecular weight CSPPC chains of CSPPC-PBAT exhibit reduced entanglement molecular weight and diminished physical crosslink density, enabling greater segmental mobility and strain accommodation, providing more impact resistance in high-performance adhesives, albeit at the cost of the ultimate tensile load capacity.

To further evaluate the adhesion performance of the CSPPC-based adhesives, the adhesion strengths of CSPPC and CSPPC-PBAT were compared with those of previously reported adhesives, as shown in Fig. 6. Relative to previously reported bio-based alternatives, our CSPPC-35-PBAT adhesive system exhibits superior bonding performance. First, when benchmarked against adhesives such as RADX-1.5, PESF, MTAG0.42, ET0.4C0.6, BSA, and PBDF, our material achieves a shear strength of 14.23 MPa on stainless steel, substantially exceeding their values. Second, relative to CPPC-based adhesives, our CO_2-derived PPC *via* gas-solid chlorosulfonation is more environmentally benign. Notably, even un-extended CSPPC-35 gives 6.35 MPa, higher than CPPC counterparts, and extension with PBAT raises it to 14.23 MPa. Overall, our system offers high strength and green synthesis.

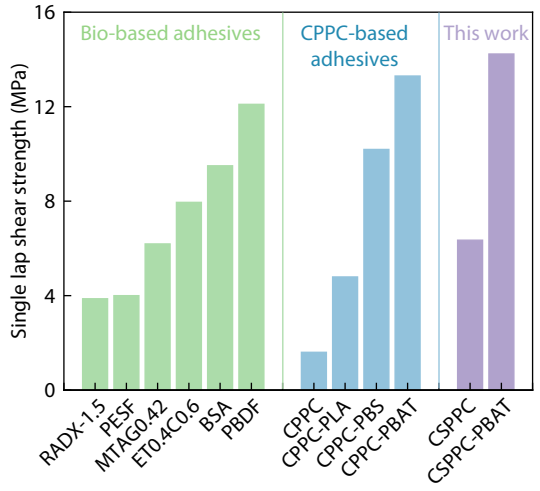


Fig. 6 Comparison of the single lap shear strength of CSPPC and CSPPC-PBAT adhesives on stainless steel with that of reported adhesives (bio-based adhesives: RADX-1.5,[21] PESF,[26] MTAG0.42,[40] ET0.4C0.6,[41] BSA,[42] PBDF;[43] CPPC-based adhesives: CPPC,[35] CPPC-PBAT,[35] CPPC-PLA[33] and CPPC-PBS[44]).

The Viscoelastic Behavior of Chain-extended CSPPC-PBAT and the Adhesion Performance as HMAs

To systematically elucidate the molecular-weight-dependent regulation of thermomechanical properties in chain-extended CSPPC hot-melt adhesives, a series of CSPPC-PBAT samples were characterized by oscillatory shear rheology with temperature sweeps (Fig. 7). Relative to the unmodified CSPPC precursor (Fig. 3), both the G' and G'' of the chain-extended CSPPC-PBAT exhibited substantial increases. This enhancement can be attributed to the introduction of rigid terephthalic acid units within the PBAT segments, which effectively increased the chain rigidity and intersegmental interaction energy, thereby elevating the cohesive strength of the system, which is consistent with the tensile mechanical property data (Figs. 5e and 5f). Simultaneously, the polar ester functionalities in PBAT significantly enhanced the polar interactions and interfacial adhesion contributions, resulting in a concomitant increase in the loss modulus. Thus, the chain-extension modification of CSPPC achieves a synergistic enhancement of the elastic and viscoelastic responses in CSPPC-PBAT samples, establishing the requisite viscoelastic balance for high-performance HMA applications.

However, the enhancing effect of PBAT chain extension on the HMA properties is strongly dependent on the molecular weight of the CSPPC precursor. For high-molecular-weight systems (CSPPC-49-PBAT and CSPPC-54-PBAT), as shown in Figs. 7(a) and 7(b), the samples exhibited typical dual-platform modulus decay characteristics during the temperature scan process. Both G' and G'' showed two distinct stepwise drops, indicating the presence of microphase separation or multi-scale relaxation behavior within the system, and the segmental motion was significantly constrained. Mechanically, the excessively high molecular weight of CSPPC-54 leads to a sharp decline in the segmental motion ability, a significant increase in melt viscosity, and severe weakening of the spreading and wetting ability of the hot melt adhesive on the substrate surface. At the same time, the introduction of PBAT rigid segments may induce local crystallization or ordered aggregation structures, further restricting sufficient relaxation and interface diffusion of the molecular chains. Therefore, although the high-molecular-weight samples have higher cohesive strength, their interfacial bonding efficiency is insufficient, the processing window is significantly narrowed, and the single lap shear strength of CSPPC-54-PBAT is lower than that of the medium-molecular-weight samples, with the failure mode mainly being interface failure.

When the CSPPC precursor exhibited a moderate molecular weight (CSPPC-35-PBAT and CSPPC-30-PBAT; Figs. 7c and 7d), the resulting chain-extended samples achieved an optimal G'/G'' balance, reflecting synergistic alignment between cohesive integrity and interfacial adhesion, thereby displaying viscoelastic signature characteristics of high-performance HMAs. Notably, CSPPC-35-PBAT exhibited the broadest and most thermally robust G' and G'' plateaus, sustaining viscoelastic equilibrium across the widest temperature range among all the formulations. This rheological profile confers a dual functional advantage, high elasticity (evidenced by elevated cohesive strength) and high viscous dissipation (enabling superior substrate wetting and interfacial contact). Finally, it delivered the highest adhesion performance among all tested samples (Fig. 5a, 14.23 MPa).

Critically, the well-balanced G'/G'' ratio, with G' exhibiting exceptional plateau width and thermal stability (Fig. 7c), underpins a strong and sticky mechanical response, shifting the dominant failure mode from mixed (cohesive + interfacial) to predominantly cohesive failure, which is a property of optimized bulk energy dissipation rather than premature interfacial debonding. Therefore, these findings establish the CSPPC precursor molecular weight as the decisive structural parameter governing the HMA performance in this system. Only within a narrowly defined, molecular-weight-dependent optimum can a high modulus, robust viscoelastic balance, and ef-

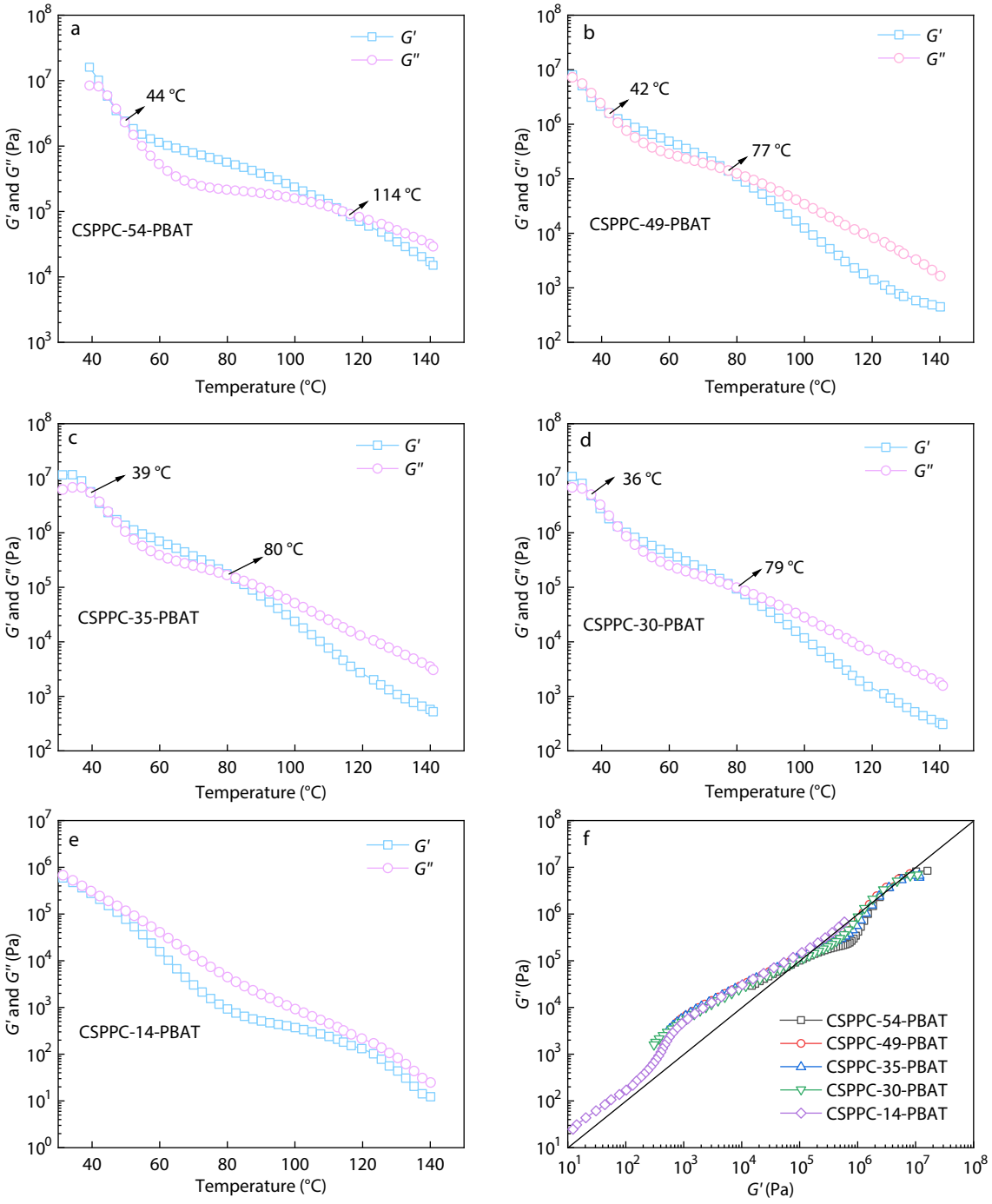


Fig. 7 Rheological properties of CSPPCs-PBAT. (a–e) Storage modulus (*G*') and loss modulus (*G*") of CSPPCs-PBAT; (f) Viscoelastic processing window of CSPPCs-PBAT.

fective interfacial coupling be concurrently achieved, thereby enabling chain-extended CSPPC-PBAT to fulfill the essential functional requirements of a high-performance, melt-processable HMA.

Conversely, for the low-molecular-weight system CSPPC-14-PBAT (Fig. 7e), *G′* remained lower than *G″* across the entire temperature range, with minimal separation between the moduli. This indicates a viscous-flow-dominated response that lacks effective elastic network support. The low molecular weight results in an extremely low chain entanglement density, a weak physical crosslinking network, and insufficient cohesive strength. Consequently, cohesive failure occurred readily during bonding, yielding the lowest adhesion performance (Fig. 5a) among all the samples, with cohesive failure as the predominant failure mode.

In summary, the CSPPC precursor exhibited a pronounced molecular-weight window effect on the performance of chain-extended CSPPC-PBAT as a hot-melt adhesive. An effec-

https://doi.org/10.1007/s10118-026-3863-7

tive physical entanglement network cannot be established at an excessively low molecular weight (14 kg/mol), resulting in an insufficient cohesive strength. At excessively high molecular weights (49 or 54 kg/mol), the restricted segmental mobility and potential microphase separation reduce the interfacial adhesion efficiency. Only within the intermediate molecular-weight range (approximately 30–35 kg/mol) is an optimal G'/G'' balance maintained across a broad temperature window, simultaneously achieving high elasticity (cohesive strength) and high viscous dissipation (interfacial wetting). This molecular-weight window effect provides a theoretical foundation and experimental guidance for the molecular design and performance optimization of CO_2-based high-performance HMAs.

CONCLUSIONS

A series of CSPPC samples with tunable molecular weights were synthesized *via* the gas-solid phase reaction of PPC with sulfuryl chloride. By precisely balancing the competing reactions of polar group introduction (chlorine and sulfur) and controlled main-chain degradation, the optimized CSPPC-35 ($\overline{M_n}$=35 kg/mol) achieved a single-lap shear strength of 6.35 MPa on stainless steel, holding power of 99 h, and peel strength of 131 N/cm, with a failure mode transition from interfacial to cohesive failure. Rheological analysis reveals that this optimal performance originates from a balanced viscoelastic response, where the storage modulus (G') and loss modulus (G'') converge at approximately 1.0×10^5 Pa, simultaneously satisfying the dual requirements of high elasticity and sufficient viscous dissipation essential for high-performance HMAs.

The chain extension of CSPPC-35 with PBAT and MDI further elevates the lap shear strength to 14.23 MPa while maintaining robust adhesion on diverse substrates, including aluminum, walnut wood, and bamboo. The molecular weight of the CSPPC precursor exhibits a pronounced window effect: only within the moderate range of 30–35 kg/mol does the chain-extended CSPPC-PBAT system achieve an optimal G'/G'' balance, yielding superior adhesion governed by cohesive failure. CSPPC-35 efficiently reacts with various biodegradable polymers, including aliphatic polyesters and polycarbonates (*e.g.*, PCL, PPC, and CPPC), confirming its versatility as a universal precursor for high-performance HMAs.

This study establishes a molecular-weight-dependent design criterion for CSPPC-based adhesives and provides a sustainable, solvent-free platform that advances CO_2-based circular economy strategies. Future efforts will focus on long-term durability assessments and industrial-scale validations to accelerate the commercial translation of this technology.

Conflict of Interests

The authors declare no interest conflict.

Electronic Supplementary Information

Electronic supplementary information (ESI) is available free of charge in the online version of this article at http://doi.org/10.1007/s10118-026-3863-7.

Data Availability Statement

The data supporting the findings of this study are available from the corresponding author upon reasonable request.

ACKNOWLEDGMENTS

This work was financially supported by the National Natural Science Foundation of China (Nos. 52433001 and 52073276).

REFERENCES

1 Liu, W.; Gong, Z.; Chen, Y. Design of interface dynamic cross-linked hybrid network with highly improved mechanical, recycling and adhesive performance. *Chem. Eng. J.* **2023**, *471*, 144598.
2 Zhang, Z.; Quinn, E. C.; Kenny, J. K.; Grigoropoulos, A.; DesVeaux, J. S.; Chen, T.; Zhou, L.; Xu, T.; Beckham, G. T.; Chen, E. Y. Stereomicrostructure-regulated biodegradable adhesives. *Science* **2025**, *387*, 297–303.
3 Shi, J.; Li, X.; Li, A.; Wei, H.; Zhang, E.; Zhang, W. Polyurethane hot-melt adhesives for strong and tough adhesion. *Eur. Polym. J.* **2025**, *228*, 113814.
4 Sun, L.; Li, K.; Xue, W.; Zeng, Z. Thermal degradation of reactive polyurethane hot melt adhesive based on MDI. *J. Adhes. Sci. Technol.* **2018**, *32*, 1253–1263.
5 Tian, Z.; Cui, L.; Du, P. Synthesis of polyurethane hot melt adhesive without solvent *via* Diels-Alder reaction. *Int. J. Adhes. Adhes.* **2024**, *129*, 103567.
6 Shi, X.; Zhang, Y. P.; Zhang, Y.; Yan, X. H.; Wang, Z. L.; Geng, J. X. Molecular design and performance of a low-temperature resistant and waterborne polyurethane adhesive. *Acta Polymerica Sinica* (in Chinese) **2025**, *56*, 644–652.
7 Kajaks, J. A.; Bakradze, G. G.; Viksne, A. V.; Reihmane, S. A.; Kalnins, M. M.; Krutohvostov, R. The use of polyolefins-based hot melts for wood bonding. *Mech. Compos. Mater.* **2009**, *45*, 643–650.
8 Kruszynski, J.; Nowicka, W.; Ahmad Pasha, F.; Yang, L.; Rozanski, A.; Bouyahyi, M.; Kleppinger, R.; Jasinska-Walc, L.; Duchateau, R. Tuning the adhesive strength of functionalized polyolefin-based hot melt adhesives: unexpected results leading to new opportunities. *Macromolecules* **2025**, *58*, 2894–2904.
9 Annighöfer, F. Reactive hot melts on the basis of polyester and polyamide. *J. Adhes.* **1987**, *22*, 109–124.
10 Sun, H.; Yang, K.; Xiang, N.; Tang, G.; Zhang, N.; Wang, C. Six-membered ring-reinforced flexible high-elongation block polyamide as strong and multi-reusable hot melt adhesive. *Constr. Build. Mater.* **2024**, *438*, 137132.
11 Qin, J.; Dou, Y.; Wen, J.; Tang, X. Facilely accessible and reusable high-performance poly(thioester amide) adhesives with exceptional versatility and environmental stability. *Adv. Mater.* **2026**, *38*, e06748.
12 Albuquerque, R. Q.; Stephan, F.; Pongratz, A.; Brütting, C.; Krause, K.; Ruckdäschel, H. Recycling of thermoplastics with machine learning: a review. *Adv. Funct. Mater.* **2026**, *36*, e09447.
13 Borrelle, S. B.; Ringma, J.; Law, K. L.; Monnahan, C. C.; Lebreton, L.; McGivern, A.; Murphy, E.; Jambeck, J.; Leonard, G. H.; Hilleary, M. A.; Eriksen, M.; Possingham, H. P.; De Frond, H.; Gerber, L. R.; Polidoro, B.; Tahir, A.; Bernard, M.; Mallos, N.; Barnes, M.; Rochman, C. M. Predicted growth in plastic waste exceeds efforts to mitigate plastic pollution. *Science* **2020**, *369*, 1515–1518.
14 Westlie, A. H.; Quinn, E. C.; Parker, C. R.; Chen, E. Y. Synthetic

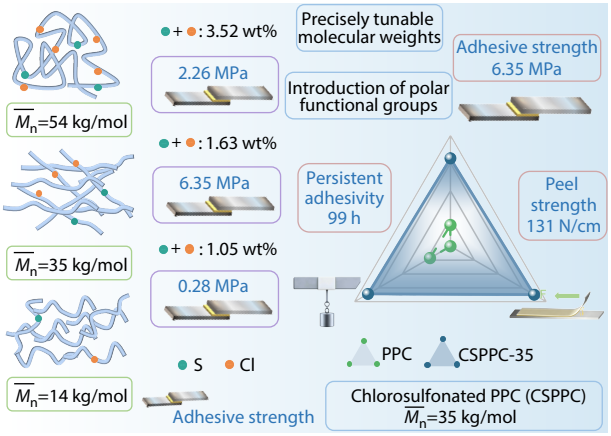
Graphical Abstract

Chlorosulfonated Poly(propylene carbonate) as High-performance Hot-melt Adhesives: Balancing Interfacial Adhesion and Cohesive Strength through Molecular Weight Window Engineering

Hai-Long Tian, Meng-Yu Yang, Hai-Ying Tan, Jing Jin, Yun-Bao Gao, and Wei Jiang

Wuhan Textile University

Gas-solid chlorosulfonation of CO_2-derived poly(propylene carbonate) (PPC) yields tunable chlorosulfonated PPC (CSPPC); optimized CSPPC-35 achieves 6.35 MPa adhesion, 131 N/cm peel, 99 h hold, establishing a sustainable hot-melt adhesive platform.



Chinese J. Polym. Sci. 2026 *https://doi.org/10.1007/s10118-026-3863-7*

biodegradable polyhydroxyalkanoates (PHAs): recent advances and future challenges. *Prog. Polym. Sci.* **2022**, *134*, 101608.
15 Luo, X.; Lauber, K. E.; Mather, P. T. A thermally responsive, rigid, and reversible adhesive. *Polymer* **2010**, *51*, 1169–1175.
16 Pal, S.; Shin, J.; DeFrates, K.; Arslan, M.; Dale, K.; Chen, H.; Ramirez, D.; Messersmith, P. B. Recyclable surgical, consumer, and industrial adhesives of poly(*α*-lipoic acid). *Science* **2024**, *385*, 877–883.
17 Westerman, C. R.; McGill, B. C.; Wilker, J. J. Sustainably sourced components to generate high-strength adhesives. *Nature* **2023**, *621*, 306–311.
18 Guo, Y. K.; Li, H.; Zhao, P. X.; Wang, X. F.; Astruc, D.; Shuai, M. B. Thermo-reversible MWCNTs/epoxy polymer for use in self-healing and recyclable epoxy adhesive. *Chinese J. Polym. Sci.* **2017**, *35*, 728–738.
19 Wu, J.; Hua, Z.; Liu, G. M. Nucleobase-tackified thioctic acid-based degradable and recyclable supramolecular polymer adhesives. *Chinese J. Polym. Sci.* **2025**, *43*, 1089–1095.
20 Zhang, H. L.; Sun, Y. Q.; Xu, Y.; Wang, L.; Li, Y.; Zhang, J.; Geng, B.; Li, S. S.; Zong, C. Y. Design of weldable and recyclable fluorine-containing adhesives utilizing dynamic-covalent boroxine bonds. *Chinese J. Polym. Sci.* **2025**, *43*, 1433–1442.
21 Lv, Z.; Yan, X.; Jia, S.; Pan, J.; Hao, X.; Chen, G.; Lü, B.; Rao, J.; Peng, F. Bio-based hot-melt adhesive from xylan. *Nat. Sustain.* **2025**, *8*, 827–836.
22 Jenkins, C. L.; Siebert, H. M.; Wilker, J. J. Integrating mussel chemistry into a bio-based polymer to create degradable adhesives. *Macromolecules* **2017**, *50*, 561–568.
23 Tian, W.; Deng, J.; Wang, H.; Zheng, J.; Zhou, Z. A hierarchical energy dissipation supramolecular elastomer with superhigh toughness and cohesive strength for adhesive applications. *Macromolecules* **2026**, *59*, 298–311.
24 Zhang, S. J.; Chen, X. X.; Cui, C. H.; Ma, L.; Zhong, Q. Y.; Shen, K. X.; Yu, J.; Li, Z.; Wu, Y. S.; Zhang, Q.; Cheng, Y. L.; He, L.; Zhang, Y. F. Strong, removable, and photoluminescent hyperbranched polyamide-amine hot melt adhesive. *Chinese J. Polym. Sci.* **2021**, *39*, 1319–1327.
25 D'Angelo, K. A.; Sun, N.; Ciccia, N. R.; Yu, I. F.; Helms, B. A.; Hartwig, J. F. Catalytic borylation of poly(vinyl chloride) produces adhesive materials. *J. Am. Chem. Soc.* **2025**, *147*, 27186–27191.
26 Jiang, W.; Wang, Z.; Fang, T.; Zhang, Z.; Zhu, W. Bio-based catalyst-free polyester hot melt adhesive. *Chem. Eng. J.* **2025**, *520*, 165876.
27 Lv, J.; Zhang, D.; Li, X.; Miao, Y.; Wang, Y.; Wang, Y.; Zhang, X. Reversible biobased adhesives enable closed-loop engineered composites. *Nat. Commun.* **2025**, *16*, 7871.
28 Zhong, K.; Guan, Q.; Sun, W.; Qin, M.; Liu, Z.; Zhang, L.; Xu, J.; Zhang, F.; You, Z. Hot-melt adhesive based on dynamic oxime–carbamate bonds. *Ind. Eng. Chem. Res.* **2021**, *60*, 6925–6931.
29 Cui, X. H.; Jin, J.; Cui, J.; Zhao, G. Y.; Jiang, W. Preparation of chlorinated poly(propylene carbonate) and its distinguished properties. *Chinese J. Polym. Sci.* **2017**, *35*, 1086–1096.
30 Inoue, S.; Koinuma, H.; Tsuruta, T. Copolymerization of carbon dioxide and epoxide. *J. Polym. Sci. B Polym. Lett.* **1969**, *7*, 287–292.
31 Zhong, X.; Dehghani, F. Solvent free synthesis of organometallic catalysts for the copolymerisation of carbon dioxide and propylene oxide. *Appl. Catal. B Environ.* **2010**, *98*, 101–111.
32 Cui, X.; Jin, J.; Zhao, G.; Jiang, W. Preparation of chlorinated poly(propylene carbonate) and its effects on the mechanical properties of poly(propylene carbonate)/starch blends as a compatibilizer. *Polym. Bull.* **2020**, *77*, 1327–1342.
33 Li, J.; Wang, D.; Jin, J.; Li, F.; Gao, Y.; Liang, H.; Jiang, W. Improving the shear and tack strengths of chlorinated poly(propylene carbonate) through chain extension with polylactic acid for biodegradable hot melt adhesives. *ACS Appl. Polym. Mater.* **2023**, *5*, 10256–10264.
34 Mao, W.; Li, J.; Wang, D.; Pan, Y.; Ji, X.; Jiang, W. Biodegradable CPPC/PBS/PLA blends with enhanced adhesive properties by *in situ* compatibilization. *Colloid Polym. Sci.* **2025**, *303*, 2179–2188.
35 Wu, M.; Gao, Y.; Sun, J.; Jin, J.; Tan, H.; Jiang, W. High-strength,

waterproof, and biodegradable adhesive based on poly(propylene carbonate) for sustainable and recycling economy. *Chem. Eng. J.* **2026**, *530*, 173449.
36 Wang, D.; Li, J.; Jin, J.; Pan, Y.; Liang, H.; Ji, X.; Jiang, W. Chlorosulfonated poly(propylene carbonate)-based pressure-sensitive adhesives with improved thermal stability and peel strength. *ACS Appl. Polym. Mater.* **2024**, *6*, 8896−8904.
37 Wang, D.; Li, J.; Li, F.; Zhang, J.; Gao, Y.; Jin, J.; Jiang, W.; Liang, H. Solvent-free and biodegradable pressure-sensitive adhesive based on chlorosulfonated poly(propylene carbonate). *Polymer* **2023**, *286*, 126418.
38 Chang, E. P. Viscoelastic windows of pressure-sensitive adhesives. *J. Adhes.* **1991**, *34*, 189−200.
39 Deacy, A. C.; Gregory, G. L.; Sulley, G. S.; Chen, T. T. D.; Williams, C. K. Sequence control from mixtures: switchable polymerization catalysis and future materials applications. *J. Am. Chem. Soc.* **2021**, *143*, 10021−10040.
40 Chen, X.; Li, X.; Li, Q.; Huang, J.; Li, T.; Wang, Y.; Wang, S.; Zhang, X.; Dong, W. A mechanically robust, multi-environmentally adaptive and solvent-free bio-based adhesive with hyperbranched structure. *Chem. Eng. J.* **2025**, *523*, 168404.
41 Zhuang, Z.; Zhang, Y.; Chen, P.; Zhang, S.; Yang, X. Preparation and properties of a fully biobased adhesive based on epoxidized soybean oil. *ACS Sustainable Chem. Eng.* **2026**, *14*, 722−737.
42 Sun, P.; Mei, S.; Xu, J. F.; Zhang, X. A bio-based supramolecular adhesive: ultra-high adhesion strengths at both ambient and cryogenic temperatures and excellent multi-reusability. *Adv. Sci.* **2022**, *9*, 2203182.
43 Wang, H.; Shi, X.; Xie, Y.; Gao, S.; Dai, Y.; Lai, C.; Zhang, D.; Wang, C.; Guo, Z.; Chu, F. A furan-containing biomimetic multiphase structure for strong and supertough sustainable adhesives. *Cell Rep. Phys. Sci.* **2023**, *4*, 101374.
44 Mao, W.; Pan, Y.; Ji, X.; Jiang, W. Preparation and properties of chlorinated poly(propylene carbonate) and poly(butylene succinate) blends as hot melt adhesives through chain extension reaction. *Polym. Bull.* **2025**, *82*, 5121−5137.

https://doi.org/10.1007/s10118-026-3863-7